International Journal of Automation and Computing 17(4), August 2020, 527-538
DOI: 10.1007/s11633-019-1217-4

Kinematic Analysis of an Under-actuated, Closed-loop Front-end Assembly of a Dragline Manipulator

Muhammad A. Wardeh[1,2] Samuel Frimpong[1]

[1] Department of Mining and Nuclear Engineering, Missouri University of Science and Technology, Rolla 65409, USA

[2] Center for Infrastructure Engineering Studies, Missouri University of Science and Technology, Rolla 65409, USA

Abstract: Dragline excavators are closed-loop mining manipulators that operate using a rigid multilink framework and rope and rigging system, which constitute its front-end assembly. The arrangements of dragline front-end assembly provide the necessary motion of the dragline bucket within its operating radius. The assembly resembles a five-link closed kinematic chain that has two independent generalized coordinates of drag and hoist ropes and one dependent generalized coordinate of dump rope. Previous models failed to represent the actual closed loop of dragline front-end assembly, nor did they describe the maneuverability of dragline ropes under imposed geometric constraints. Therefore, a three degrees of freedom kinematic model of the dragline front-end is developed using the concept of generalized speeds. It contains all relevant configuration and kinematic constraint conditions to perform complete digging and swinging cycles. The model also uses three inputs of hoist and drag ropes linear and a rotational displacement of swinging along their trajectories. The inverse kinematics is resolved using a feedforward displacement algorithm coupled with the Newton-Raphson method to accurately estimate the trajectories of the ropes. The trajectories are solved only during the digging phase and the singularity was eliminated using Baumgarte′s stabilization technique (BST), with appropriate inequality constraint equations. It is shown that the feedforward displacement algorithm can produce accurate trajectories without the need to manually solve the inverse kinematics from the geometry. The research findings are well in agreement with the dragline real operational limits and they contribute to the efficiency and the reduction in machine downtime due to better control strategies of the dragline cycles.

Keywords: Dragline mining manipulator, underactuated closed-loop mechanism, generalized speeds, Baumgarte′s stabilization technique (BST), feedforward displacement.

1 Introduction

The global increase in energy demands necessitates energy producers to develop methods and techniques that expedite the exploration and extraction of energy minerals. The strip mining method is one of these methods in the surface coal mining industry. This method is primarily used to excavate overburden (waste materials) and to expose the coal seams beneath the overburden materials. Dragline excavators play a key role in the stripping method due to their unique designs, large bulk handling capacity, and quick return on investment. Draglines are a special kind of cable driven robotic excavators that operate using wire ropes, which reel in/out on sheaves, and carry suspended loads of between 50 tons and 500 tons[1].

The ropes and rigging, boom, bucket and their support structures are termed as the front-end assembly as depicted in Fig. 1 (b). Dragline operations are cyclic in nature and include digging by dragging the bucket to excavate materials, lifting and swinging, and dumping the materials in the bucket. During the digging phase, the drag rope retracts, and the hoist rope increases in length to engage the bucket into the bench for achieving a proper filling with the materials. However, during the dumping phase, the change of rope lengths is reversed, and the machine house swings to lift and maneuver the bucket for dumping on the spoil area as shown in Fig. 1 (a).

The dragline cycle constitutes the following phases: empty-bucket swinging back, dragging bucket to excavate material, filled-bucket swinging, and dumping. It usually lasts for 60 s and that depends on the operator skills, as well as machine availability, utilization, and bucket filling efficiency.

Several researchers have investigated the dragline performance and developed models to monitor its key performance indicators (KPIs). KPIs are critical parameters for defining the dragline mining efficiencies, including mine production targets, reliability of equipment, and maintenance schedules, workplace safety and health[2]. For example, dragline suspended load can be monitored instantly to ensure that the operator runs the machine within its limits. Other KPIs include, but are not limited to, bucket pose, swinging angle, and sequence of operation[3]. Kemp[4] used an on board sensor monitor that tracks machine variables, such as total power consumption, hoist and drag ropes wear index, and swinging

Research Article
Manuscript received May 20, 2019; accepted December 18, 2019; published online March 5, 2020
Recommended by Associate Editor Min-Cheol Lee

(a) Physical model (Komatsu[1], 2019)

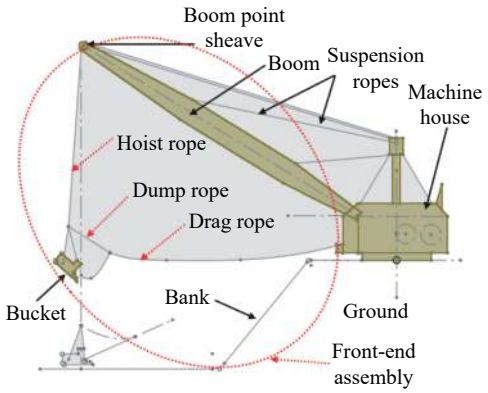

(b) Dragline nomenclature

Fig. 1 Dragline model 9020

angle. A minicomputer is used to print out data on production and delays and serves reducing power consumption per unit cost of operation.

McCoy Jr. and Crowgey[5] designed static and dynamic anti-tight line control systems that use signals derived from the rope′s variable lengths and speeds. The systems can control the bucket movement and provide corrective actions that prevent it from colliding with the machine. Godfrey and Susanto[6] developed mathematical models that describe the static and dynamic characteristics for the hoist, drag, and swing drive systems. Characteristics that pertain to the hoist and drag drive include magnetic and electrical models for the generators and motors, electrical torque generation, mechanical losses, inertia and forces in the ropes. The characteristics of the swing drive include variable inertia, inclination of the tub of machine house, pendulum effect of the bucket, but not those Coriolis and centrifugal forces. The kinematics analysis showed a general agreement with the physical model. However, these mathematical models cannot be elaborated in further analysis due to the limitations of stated assumptions.

A dragline machinery weighs from 500 to 13 500 metric tons and its boom length ranges from 100 ft to 400 ft. A dragline is a very capital-intensive investment for overburden stripping in surface coal mining operations with very high operating costs[7]. This equipment can only be designed and fabricated upon a customer request. Its productivity, the amount of materials moved per hour (bucket size/hour) and the operating cost per ton ($/tons), is greatly impacted by poor mining process, unscheduled maintenance, and breakdowns. There are also multiple factors that affect the dragline productivity, such as cycle time, bucket size, availability, and utilization. Different scaled physical prototypes were developed in order to measure the effect of each factor on the productivity.

Haneman et al.[8] performed multiple physical testing on small-scale and large-scale buckets to assess its effect on the performance. The authors found that large-scale models do not affect the filling behavior, but they improve the productivity when compared to the field data. Esterhuyse[9] investigated the effects of bucket geometry on the filling behavior using a scaled down, physical prototype of a dragline. His findings indicate that filling behavior is the same for different bucket geometries. Knights and Shanks[10] reported an increase of the dragline productivity by 2% with the aid of short-term monitoring of a dragline bucket. Corke et al.[11] and Roberts et al.[12] tested a physical prototype of a dragline. The authors used a real-time kinematic (RTK)-GPS receiver to track the operations of a dragline and with a 3D digital map terrain, they were able to perform 50 autonomous cycles.

Kyle and Costello[13] constructed a 1/16-scale dragline physical prototype to capture the dynamic effects in the bucket during digging. They also formulated a simplified analytical model that uses discrete element ropes and three Euler angles for the bucket orientations. Their model has shown good agreement for the bucket motion and rope lengths, except for the bucket and hoist pitch dynamics due to unmolded damping effects. Yang et al.[14] developed a dynamic model for a ship-mounted crane with an adaptive anti-swing control. The controller design uses a double-layer neural-network structure to handle issues associated with dead zones and unidirectional input constraints. Lyapunov-based functions are used to prove the stability of the system and the convergence of the payload swing angle. According to the authors, payload swing is suppressed to zero degrees and the rope positioning is achieved in a finite time.

Yang and Tan[15] designed a sliding mode control scheme to control the position of a single flexible-link manipulator based on an adaptive radial basis function (RBF) neural network. The authors used Lyapunov′s method based on an infinite dimensional model to ensure the stability of the closed-loop system. Zhang et al.[16] developed second-order sliding mode controllers and fixed-time disturbances observer for a 5 degrees of freedom (DOF) exoskeleton robot. The stability of position and velocity subsystems are analyzed using Lyapunov theory. According to the authors, these designs achieve fast convergence and excellent tracking performance.

In the recent developments in the power devices, the dragline control has evolved more and new adaptive parameter identification with predictive control techniques are used in active front end (AFE) rectifiers[17]. Liu et al.[18]

used computed torque control (CTC) and robust control (RC) approaches to control the arm of a hydraulic excavator. The authors show that the RC reduces the tracking error and improves the excavator performance. Niu et al.[19] applied an adaptive sliding mode control (SMD) to handle the stability issues in a three degrees of freedom parallel manipulator with actuation redundancy. The authors claim a substantial improvement in the trajectory of the end-effector when the controller is coupled with a synchronization error.

Demirel and Frimpong[20] used a vector approach and simultaneous constraint method (SCM) to construct a two 2D planar kinematic model of dragline during the digging phase. However, their model is limited to a 6-link closed kinematic chain and the bucket and its rigging are modeled as a single rigid element. Li and Liu[21] formulated a 3-link closed chain kinematic model of a dragline using a vector approach and SCM. The bucket and its rigging as well as the boom sheave are modeled as a point mass.

Research findings using the mathematical formulations of dragline kinematics immensely contribute to the body of knowledge and provide a basis for better machinery design and analysis. Unfortunately, these studies and their results do not capture a real-world representation of the dragline front-end assembly, nor do they provide accurate measures of the kinematics and dynamic behaviors in a 3D operational space. For example, the exclusion of a heavy mechanical element adversely impacts the results. Moreover, the lack of field data and use of simplified physical models make the kinematics and dynamic analysis unrealistic. Thus, it is critical to formulate a new kinematic model of a dragline robotic excavator that can realistically capture the real dragline kinematics during its operational cycle, overcome the shortcomings of previous models, and improve mining machinery design and analysis.

This paper presents a new kinematics formulation of dragline kinematics using the concept of generalized speeds from Kane method in Kane and Levinson[22]. The kinematics model is a 3 DOF model that captures dragging and swinging motions of the bucket in a 3D working space. The model accounts for the excluded components of the front-end assembly such as boom sheave, rigging system, sliding effect of the bucket. Once the kinematics model is formulated, the solution is sought using a feedforward solution algorithm. Then, the solution approach is analyzed against singularity using a minimal set of constraint equations. Finally, the linear and angular displacements of ropes and bucket are plotted and verified against field data.

2 Geometry of the dragline front-end assembly

Dragline is a massive mining equipment, whose unique design allows excavating, hauling, and dumping waste materials in a cyclic nature within the mine area. Fig. 1 shows a dragline with a tabular structural steel boom pinned in its foot to the machine house and holds a boom-point sheave at its farthest end. The boom is fixed at an angle of 30° to 40° using galvanized bridge-strands. The machine house sits on a tub with rollers and can rotate 360° around an axis, which passes through the center of its tub. The house contains electric drives for swinging, hoisting, dragging, and propelling, as well as the operator cabin. The machine house (B)[1], boom (C), boom sheave (D), ropes (E, F, G and H), and bucket (H_1) constitute the front-end assembly as shown in Fig. 2.

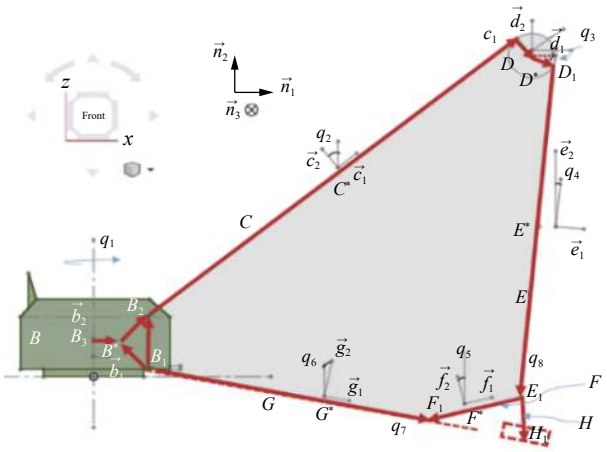

Fig. 2 Dragline kinematics diagram and its vector loop closure

The kinematics modeling is carried out under the following assumptions:

1) The inertia reference frame is fixed in a Newtonian reference frame N.

2) Swinging axis is coincident with $\vec{b}_2$. It is, however, not coincident with the machine house center of mass (COM). This allows capturing the inertia effect during swinging motion.

3) Machine house, boom, ropes, and chains are inextensible and rigid. Hoist and drag ropes are, however, changeable in length and weight in reaction to the duty cycle of the machine.

4) Angular displacements of each element in the loop is measured from y-axis and is positive if the link rotates clockwise.

5) The machine house has already made an angular displacement of $q_1.\vec{b}_2$ to position the bucket in front of bank to start the excavation process.

6) Linear velocities of drag and hoist ropes as well as swinging displacement are known.

Machine house height is modeled as a vector $(\overrightarrow{B_1B_2})$,

[1]The machine house is not part of the front-end assembly, but it has been incorporated into the model to create a robust model framework.

and is followed by the boom whose length vector is $\overrightarrow{B_2C_1}$ and is inclined by a constant angle (q_2) with respect to a global reference frame $\vec{n}_i$. The boom-sheave interaction is represented by vector $\overrightarrow{C_1D^*}$. The orientations of the hoist, dump, and drag ropes are not constants and are defined by q_4, q_5 and q_6, respectively. The dump rope $\left(\overrightarrow{E_1F_1}\right)$ has a fixed length during filling and full bucket swinging phases. During the digging phase, the position and orientation of the bucket are defined by the vector $\left(\overrightarrow{E_1H_1}\right)$ and the angle (q_5), respectively. During the full-bucket swinging phase, its motion and orientation are defined by angles (q_4, q_5, q_6, q_7 and q_8).

3 Kinematic model of the front-end assembly

The productivity of any excavator is a measure of the amount of materials being excavated and moved in tons per hour. This productivity is driven by a trajectory that the bucket should follow within machine reach and mine constraints. This motion resembles the orientations and paths that a rigid multilink robot end-effector must follow from an initial position to a desired one in order to reach the required productivity. However, this path planning is not trivial in a case of a multilink robot-like excavator that has ropes or cables. The search for an optimal path that meets productivity targets becomes a challenging task, especially when the system is a type of under-actuated closed loop mechanisms. The under-actuated closed loop mechanism has fewer inputs than the number of DOFs. For these mechanisms, if the solution is to find the joint space angles for a given bucket pose, the analyst would then attempt to exclude some important components in the mechanism. Consequently, this exclusion reduces the accuracy of the model and its capability of reflecting the real motion.

The solution approach starts with the definition of a set of constraint equations that guarantee loop closure of the front-end assembly. Numerical procedures are developed with the aid of user-defined functions in Mathematica. At the beginning of digging, the configuration constraint equations are first solved in order to find the initial conditions of the ropes and bucket trajectories. Input data for the mathematical models are given in Table 1 for a Marion 7 800 dragline and parameter notations are given in the Appendix (Table A1).

3.1 Configuration constraint equations

Fig. 2 shows the closed-loop mechanism of the dragline front-end with three independent generalized coordinates q_1, q_4 and q_6 and three dependent ones q_5, q_7 and q_8. Generalized coordinates q_1, q_7 and q_8 represent the angular displacement of the machine house, linear displacement of the drag rope and linear displacement of the hoist rope,

Table 1 Input data for the mathematical model

Parameter	Value (m)	Parameter	Value
L_0	7	L_{11}	2.29 (m)
L_1	10.76	L_{12}	7.14 (m)
L_2	10.76	L_{13}	7.14 (m)
L_3	7.95	R_s	1.715 (m)
L_4	7.95	D1E1	q_8 (m)
L_5	45.7	B1F1	q_7 (m)
L_6	45.7	E1F1	10.5 (m)
L_7	1.715	B1D	110 (m)
L_8	1.715	ca	$5\pi/180$
L_9	5.25	q_2	$32\pi/180$
L_{10}	5.25	λ	$37\pi/180$

respectively. These entities are known functions of time, and they are defined from the field observations of the machine during operation. For example, the linear displacements of the hoist and drag ropes during digging are $2.54t$+75 and $-1.32t$+75, respectively. The negative sign indicates the drag rope is retracted during digging. The loop must satisfy the configuration constraint equations as provided in (1) and (2) and an additional (3) defined by an imaginary link D_1F_1.

$$(L_5+L_6)\,c_2+L_7s_2+L_8c_4- q_8s_4-(L_9+L_{10})\,c_5-q_7c_6=0 \tag{1}$$

$$L_0+(L_5+L_6)\,s_2-L_7c_2-L_8s_4+ q_8c_4-(L_9+L_{10})s_5+q_7s_6=0 \tag{2}$$

$$-11\,986.81+220c\left(\frac{37\pi}{180}+q_6\right)q_7-q_7^2+ q_8^2-21c\,(1.57+q_4+q_5)\sqrt{2.94+q_8^2}=0. \tag{3}$$

Equations (1)–(3) are nonlinear, non-differential algebraic equations (AE) and are commonly found in the kinematics analysis of mechanisms or robots. These equations must be converted from AE to differential algebraic equations (DAE) by taking the first differentiation with respect to time. L_i denotes the length of the i-th link in the front-end assembly and c_i and s_i are the abbreviations of the trigonometric functions Sin and Cos.

It is worth noting that the type of the mechanism and the functionality of its links affect the structure of the constraint equations. In other words, when a mechanical system has a closed-loop mechanism of many rigid and flexible links, it will be very difficult to establish a geometrical relationship among them. For example, Fig. 3 (a) shows the same model with the vector loop of interest shown in dotted-line vectors, but some vectors are assembled to facilitate the analysis. However, this loop is

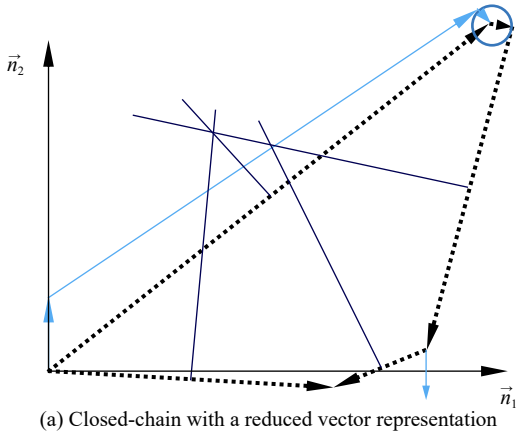

(a) Closed-chain with a reduced vector representation

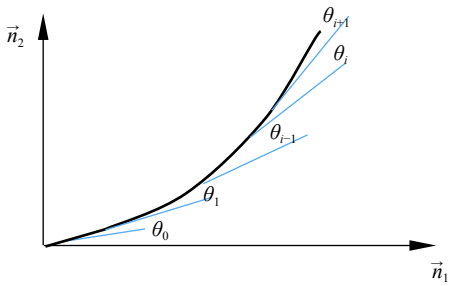

(b) Drag rope representation using finite segment approach

Fig. 3 Kinematic modeling of the dragline closed-loop

not a pentagon shape because it does not have the properties of pentagon. Therefore, (3) is necessary to complement the analysis and interrelate the generalized coordinates.

From Fig. 3 (a), it can be seen the wire flexibility is not included in this kinematics model. This assumption is valid during the digging phase and is based on the shapes of hoist and drag ropes. Field observations show that the hoist rope is straight under the effect of bucket weight, as well as the drag rope under the effect of direct tension provided by the drag motors. After filling the bucket, the operator partially releases the drag clutch and fully engages the hoist motors, which allow the drag rope to sag. Rope flexibility can be modeled using finite segment or finite element approach, or by introducing component model representation with cubic polynomial shape functions. The first method relies on discretizing the rope into a finite number of rigid links with torsional springs at nodes between two elements, as shown in Fig. 3 (b), while the second approach depends on selecting modal displacements and modal coordinate matrices whose elements are a function of position vectors and time. For the first method, it is suggested to lump the masses at nodes to eliminate the effect of rigidity of links. The stiffness, at the first discretized point, can be calculated by equating the bending moment at that point subject to a tip load P to the restoring moment of spring at joint, Banerjee[23]. For joint 1, at distance x, the stiffness coefficient κ of spring and the deflection can be found as given in (4) and (5):

$$\kappa_1 \theta_1 = P\,(nL - x) \tag{4}$$

$$\theta_1 = \frac{\delta_2}{L} \tag{5}$$

where δ_2 is the deflection at joint 2 of the rope, which can also be computed using the linear beam theory as given in (6).

$$\delta_2 = \frac{P}{6EL} x^2\,(3nL - x)\,. \tag{6}$$

Now, for the i-th joint, the relative rotation of θ_i can be calculated using the finite difference method, as given in (7).

$$\theta_i = \frac{(\delta_{i+1} - 2\delta_i + \delta_{i+1})}{L}. \tag{7}$$

There are other different approaches to deal with the rope flexibility and this topic is out of the scope of this paper.

3.2 Initial condition search

The configuration constraint equations resulting from loop closure are a set of nonlinear, non-differential algebraic equations that cannot be solved without differentiation. Thus, to solve the kinematics and dynamic equations of the dragline front-end assembly, these equations must be differentiated and integrated at every time step. By taking time derivatives of equations (1)–(3), the equations take a matrix form and are given in (8).

$$\begin{bmatrix} (75+2.54\,t)\,c_4 - 1.715\,s_4 & 10.5\,s_5 & (75-1.32\,t)\,s_6 \\ -1.715\,c_4 - (75+2.54\,t)\,s_4 & -10.5\,c_5 & (75-1.32\,t)\,c_6 \\ Z_6 & Z_6 & Z_7 \end{bmatrix} \times \begin{bmatrix} \dot{q}_4 \\ \dot{q}_5 \\ \dot{q}_6 \end{bmatrix} = \begin{bmatrix} -1.32\,c_6 - 2.54\,s_4 \\ -2.54\,c_4 + 1.32\,s_6 \\ Z_8 \end{bmatrix} \tag{8}$$

where Z_6, Z_7 and Z_8 are intermediate variables, which can be written as

$$\begin{aligned} Z_6 &= 21\sqrt{2.94 + (75 + 2.54t)^2}\,s\,(1.57 + q_4 + q_5) \\ Z_7 &= 220\,(75 - 1.32t)\,s\left(\frac{37\pi}{180} + q_6\right) \\ Z_8 &= 2.64\,(75 - 1.32t) + 5.08\,(75 + 2.54t) - \\ &\quad \frac{53.34\,(75 + 2.54t)\,(1.57 + q_4 + q_5)}{\sqrt{2.941 + (75 + 2.54t)^2}} - \\ &\quad 290.4c\left(\frac{37\pi}{180} + q_6\right) \end{aligned}$$

where $\dot{q}_i$ is the time derivative of the i-th generalized coordinate. By inspecting (8), one can see that linear displacements of ropes are also included. The solution is achieved by integrating (8) at interval $[0, t_{dig}]$ using a good guess of trajectories q_4, q_5 and q_6. Equation (8) will have a solution only when the Jacobian, is a full rank matrix. If the Jacobian is rank deficient, singularity will result during the integration. Singularity means that two or more links in the mechanism are coincident and the mechanism becomes very stiff. For more details about the constraint equations and initial conditions search, refer to Wardeh[24].

3.3 Singularity of the dragline front-end mechanism

Singularity is a common issue in the kinematics analysis of multibody systems when integrating a set of nonlinear, constraint differential equations at time interval $[0, t]$. During the integration, the step size becomes very small at the singular position and the algorithm fails to converge to a solution with a minimal error. Singular positions can be found by setting the determinant of the Jacobian matrix to zero. From a geometrical point of view, the singularity of a dragline closed-loop can result when the drag and dump ropes are coincident, either making 0 or 180°, as shown in Fig. 4.

Singularity can be eliminated by applying appropriate numerical constraints to the solution algorithm. However, adding more constraints to the solution space would make the numerical model stiffer and may not lead to a quick solution. Thus, one must carefully bound some parameters that greatly affect the solution to upper and lower bounds. This approach is equivalent to an optimization method with inequality constraints. For example, the kinematics constraints, which are the limits of the lengths of both hoist and drag ropes, are added to the solution algorithm and they become inequality constraints as per (9).

$$\left.\begin{aligned} 61.67 \le q_7 \le 75.00 \\ 75.00 \le q_8 \le 100.18 \end{aligned}\right\} \tag{9}$$

where q_7 and q_8 are the linear displacements of the drag and hoist ropes, respectively. These are given functions of time.

Starting the integration with a set of initial conditions, $q_{4.1}[0] = \dfrac{10\pi}{180}$, $q_{5.1}[0] = \dfrac{30\pi}{180}$, and $q_{6.1}[0] = \dfrac{-30\pi}{180}$, whose values do not violate the machine's limits, it was seen that singularity appears at $t = 1.52$ s of the integration time as shown in Fig. 5 (a). It can be concluded that this guess estimate makes the system stiffer and affects the solution progress of the numerical solver. Integrating (8) at interval $[0, 10]$ s was performed successfully using zero initial conditions of trajectories q_4, q_5 and q_6 as giv-

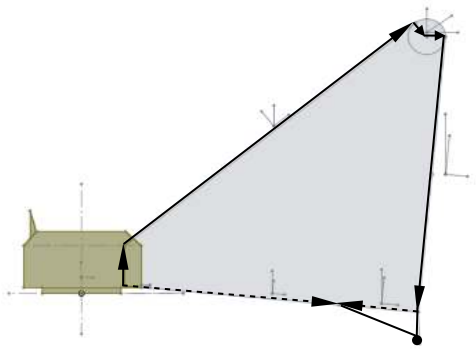

(a) Digging phase

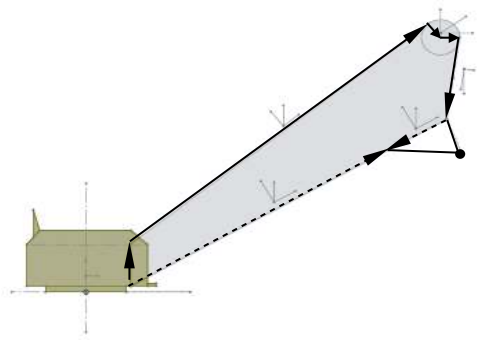

(b) Full-bucket hoisting phase

Fig. 4 Singularity positions of dragline front-end structure

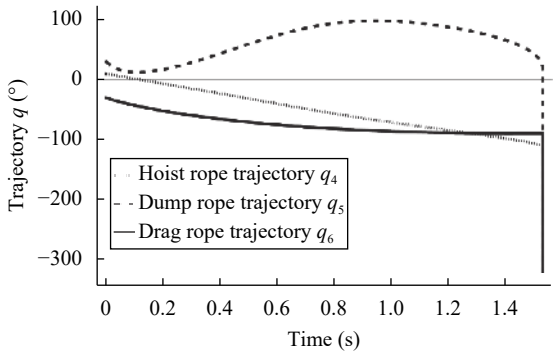

(a) Singularity issue at 1.52 s

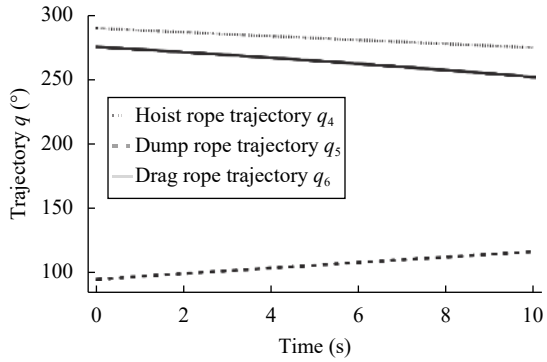

(b) Incorrect values of trajectories

Fig. 5 Trajectories of hoist, dump, and drag ropes versus time during digging phase

en in Fig. 5 (b). The singularity problem was not an issue, but these trajectories are not bounded to the operational limits of the machine. Making the search space unbounded with zero initial guess of trajectories leads to a violation and undesirable evolution of the trajectories over time. The reason is that, in the next step of the solution, the algorithm quickly tries to find consistent initial values to reduce the residual error. In addition, the initial conditions must be consistent and must satisfy constraint equations and their derivatives. It is, therefore, recommended to provide consistent initial conditions for all variables and their time derivatives.

From these experiments, it can be concluded that there is a trade-off between the initial value search and numerical stability of the applied method. In addition, the resulting trajectories are not consistent with the real-world dragline kinematics due to the presence of hidden constraints upon differentiation of (8). The hidden constraints are shown in the right hand side (RHS) of (8) and they can be determined using the second term in the RHS of (10).

$$\frac{\mathrm{d}}{\mathrm{d}t}\left(F_j\left(q_i\left(t\right),t\right)\right) = J\left(q\left(t\right),t\right).\dot{q}\left(t\right)+h_t\left(q\left(t\right),t\right) = 0. \quad (10)$$

Further differentiation will accumulate the numerical error due to the generation of additional hidden constraints as shown in (11).

$$\frac{\mathrm{d}^2}{\mathrm{d}t^2}\left(F_j\left(q_i\left(t\right),t\right)\right) = J\left(q\left(t\right),t\right).\ddot{q}\left(t\right) + J_q\left(q\left(t\right),t\right).\left(\dot{q}.\dot{q}\right) + h_{tt}\left(q\left(t\right),t\right) + 2h_{tq}\left(q\left(t\right),t\right) = 0$$

$$\begin{aligned} J_q\left(q\left(t\right),t\right) &= \frac{\partial J\left(q\left(t\right),t\right)}{\partial q} \\ h_{tt}\left(q\left(t\right),t\right) &= \frac{\partial\left(h_t\left(q\left(t\right),t\right)\right)}{\partial t} \\ h_{tq}\left(q\left(t\right),t\right) &= \frac{\partial\left(h_t\left(q\left(t\right),t\right)\right)}{\partial q}. \end{aligned} \quad (11)$$

4 Solution approach

4.1 Baumgarte's stabilization technique (BST)

To overcome the stability issue of the numerical solver and to improve the accuracy of the results, the integration must include constraint (8), as well as their first-time and second-time derivatives as per equations (10) and (11). This inclusion is called the Baumgarte's stabilization technique following Baumgarte[25] and is given by (12).

$$\ddot{F} + \alpha_B.\dot{F} + \beta_B.F = 0 \quad (12)$$

where α_B and β_B are parameters defined by the user and must meet the following rule, as given in (13):

$$\alpha_B \geq 0 \;\&\; {\alpha_B}^2 = 4\beta_B. \quad (13)$$

The benefit of using BST is the reduction of the numerical error from the hidden constraints at velocity and acceleration levels. As will be seen in the next section, the application of Baumgarte's technique solves the system singularity problem and improves the accuracy of the resulting trajectories.

4.2 Feedforward displacement algorithm

The productivity of a dragline excavator depends on the capacity and trajectory of its bucket, cycle time, and other factors. A reduction in cycle time, by some seconds, can result in significant production increases with reductions in production costs. The operations, therefore, must be performed using robust control schemes, which guarantee a short path and an effective filling of the bucket. Accurate bucket motion planning requires solving the inverse kinematics problem of the closed-loop of the dragline front-end assembly. The inverse kinematics analysis resolves the unknown rope trajectories, which are required in order to move the bucket through a desired path. It is just a mapping between task space velocities of bucket (end effector) and ropes angular velocities (joint velocities). This definition is already shown in (8) and it requires a substantial work for the kinematics model shown in Fig. 2. Instead of building an inverse kinematics using closed loop geometry, it is possible to derive the trajectories using the following scheme based on the Newton method in Mathematica:

1) Input: List of constraints algebraic equations $G(q_i) = 0$, kinematics model parameters, bucket trajectory based on q_7 and q_8

2) Initialize: trajectories q_4init, q_5init and q_6init

3) Define a trajectory vector:
q_4={}, q_5={}, and q_6={}

4) Setup: start time t_0, end time t_{final}, time increment dt, and max-error

5) Loop:

While $\{t_0 < t_{final}$ do

Setup max rotational displacement to $\frac{\pi}{2}$;

Find Root: q_iinit = Solve $\{G(q_i(t = t_0))\}$ using Newton method

Update $q_4init = q_4(t_0)$, $q_5init = q_5(t_0)$, and $q_6init = q_6(t_0)$

Find the reminder of $qinit$: $qinit$ = Mod$[q_iinit, \frac{\pi}{2}]$

Update $q_4Trjct = q_4(t_0)$, $q_5Trjct = q_5(t_0)$, and $q_6Trjct = q_6(t_0)$

maxerror1= Max[Abs$[G(q_i(t)) = 0]$, $t = t_0]$; $t_0 = t_0 + dt$;

If maxerror1 > max-error

max-error = maxerror1;

}

Interpolate: $q_i Interp$ = Interpolation[$q_i Trjct$, Interpolation Order]

If $q_i$min < $q_i Interp$ and $q_i Interp$> $q_i$max

$q_i = q_i Interp$;

Else

Replace the constraint equations $G(q_i) = 0$ by the equation (12)

Redo Step 5

6) Plot: Output q_i and maxerror1

If the algorithm outputs interpolated trajectory functions, whose values are not consistent with the machine's operational limits, the structure of the constraint equations or the initial trajectory guess must be changed to satisfy consistency conditions. The output of the solution algorithm is used directly to calculate the velocities and accelerations of the links. These kinematics entities can be used to compute forces and torques that actuate the dragline front-end mechanism.

A solution of the kinematics model can also be performed using neural networks, which are usually trained against field data to provide acceptable values of trajectories. However, their application can result in over-fitting and requires model regularization or simplification. Over-fitting is not an issue in the solution algorithm due to the robustness of the kinematics model, selection of appropriate initial conditions based on machine operational limits, application of penalty constraints of ropes trajectories and the ability to converge to a solution with minimal residual. The trajectories do not necessarily increase/decrease at the same rate at each cycle operation, but they must be consistent with machine's limits. In some cases, at the beginning of digging, the operator may throw the bucket in zones beyond the boom point sheave or accelerates the bucket during the filling. Therefore, there is no unique solution for the trajectory's evolution with time. As a result, it is not recommended to solve this model using machine learning techniques.

The solution algorithm takes only 2.125 s to compute the initial values of the trajectories of the ropes and 1.095 s to evaluate the trajectories over 10 s of digging. The machine used for the computation is an 8 Gb RAM personal computer and has an Intel Core (TM) i7-4710HQ CPU at 2.5 GHz. That confirms the robustness of the solution algorithm and the efficiency of using Baumgarte's stabilization technique (BST) to reduce the error.

5 Results and discussions

5.1 Verification of the solution scheme

Although the inverse kinematics is solved directly from joint constraint equations and their first and second derivatives, at the velocity and acceleration levels, it is necessary to verify the model against resulting errors. The kinematics model also must generate acceptable trajectories that meet the machine's operational limits. These limits are determined by the fixed structures, maximum reach of the bucket, as well as dynamics loading on the dragline structural components. The constraint (1)–(3) can be chosen as system invariants for calculating the numerical tolerance. The invariant means that the system properties do not change within time due to an external disturbance. Since these equations serve as a mathematical model that defines the geometric relationship among the links, their variations must be within the machine's design standards.

Fig. 6 shows the plots of the numerical errors that resulted from the violation of the geometric constraint equations. The absolute error of each variable (q_4, q_5 and q_6) is retuned at the end of each numerical experiment. It can be seen that the trajectory's absolute error in each of the hoist and dump ropes is well bounded, but the drag rope trajectory error increases with time and has the maximum value at 5 s. It can be noticed that the errors of all trajectories are less than 10^{-4} degrees, which proves the accuracy of the kinematics model and the robustness of the solution scheme.

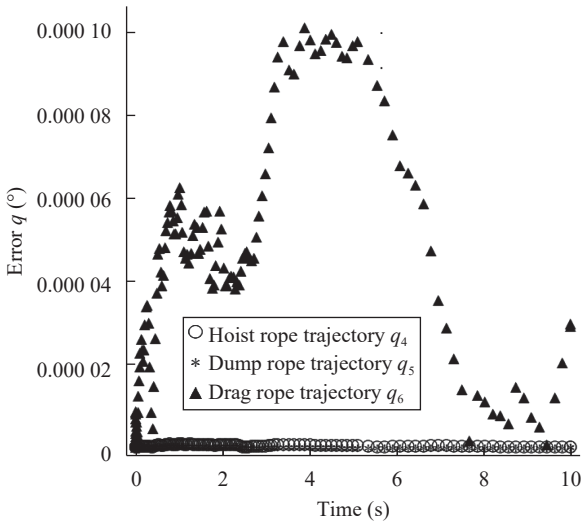

Fig. 6 Absolute errors in the trajectories of ropes of the front-end assembly

5.2 Verification of the machine operational limits

Fig. 7 shows the trajectories generated using the BST for two sets of parameters α_B=1 and β_B=0.25 and α_B=6 and β_B=9. From experiments, it was noticed that small values of the parameters improve the results, whereas the higher values tend to destabilize the algorithm. This behavior is due to the structure of the constraint equations and their derivatives, which are solved together as given by (8). It can be seen that $\alpha_B = 1$ and $\beta_B = 0.25$ minimize the influence of configuration constraint equations,

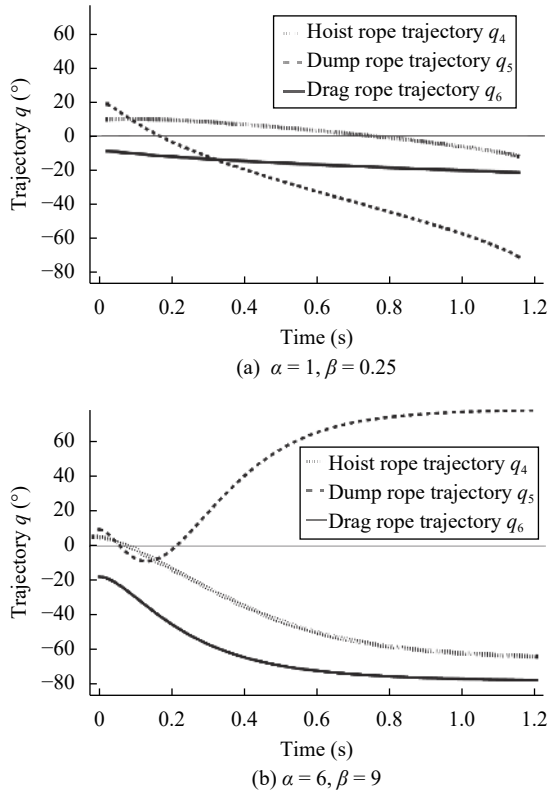

Fig. 7 Trajectories of ropes using Baumgarte′s stabilization technique (BTS) during digging phase

while it does not change the velocity equations. These values resulted in trajectories that follow a real behavior and meet the machines operational limits as shown in Fig. 7 (a). For example, after 1 s of digging, there is initial tension in the hoist rope due to its self-weight and bucket weight. And, the operator has already engaged the drag motor clutch to correctly position the bucket against the bank. These actions control the orientations of the ropes with respect to the vertical axis in their local reference frame. Consequently, the hoist and drag ropes make –10° and –20°, but the dump rope has already made –60° since it has more mobility than the other ropes.

Fig. 7 (b) analyzes the effect of selecting higher values of Baumgarte′s parameters on the solution accuracy. These trajectories are not representative of the angular motions of the dragline ropes. Also, there are no quick variations in rope displacement at short interval [0, 1] s. Thus, BST does not improve the simulation results when bigger value parameters are used in the model. However, the technique may work efficiently with the selection of higher values in different mechanisms. The initial conditions of the rope′s angular displacements and their velocities are listed in Table 2.

5.3 Validation of the kinematics model

The kinematics model of the dragline′s closed-loop mechanism must also be validated against the real-world

Table 2 Initial angular displacements and angular velocities of ropes

Rope	Initial angle (rad)	Initial velocity (rad/s)
Hoist rope	$q_4[0] = -0.0437$	$\dot{q}_4\,[0] = 0.0$
Dump rope	$q_5[0] = 0.2831$	$\dot{q}_5\,[0] = 0.0$
Drag rope	$q_6[0] = -0.4692$	$\dot{q}_6\,[0] = 0.0$

data. The numerical simulations are performed during the digging phase to predict the evolution of ropes trajectories with time. Fig. 8 (a) shows that both hoist and drag ropes have initial length of 75 m at the beginning of digging when the bucket is empty. As the bucket engages the bank, the hoist rope reels out and the drag rope is paid out by engaging the drag motor clutch and releasing the hoist motor clutch. The operator performs these actions simultaneously to avoid toppling the bucket and to guarantee a proper filling behavior. In the course of digging, the bucket becomes partially submerged in the bank and slides on the digging face. This control, from the operator, makes the hoist rope longer to reach a maximum length of 100 m and a maximum angular displacement of –27° at 10 s as given in Fig. 8 (b). However, the drag rope becomes the shortest of 61 m when it has already made a maximum angular displacement of –65° at 10 s.

The bucket and its rigging system have a trajectory

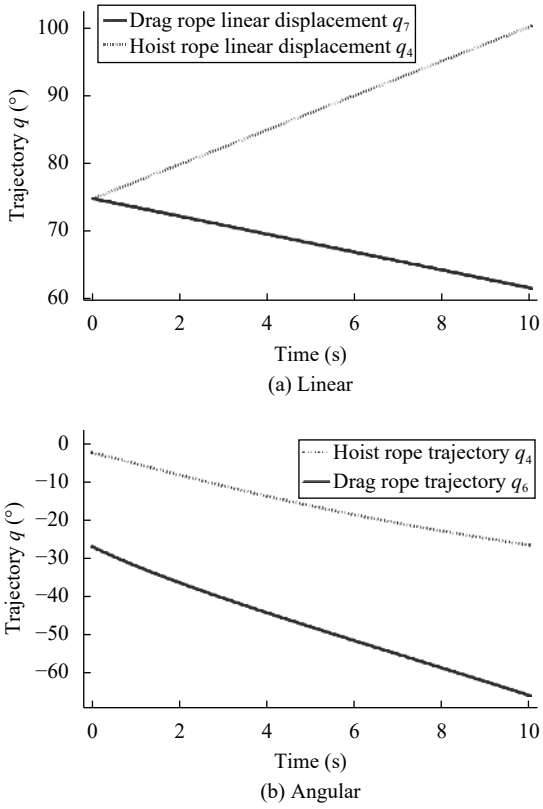

Fig. 8 Displacements of hoist and drag ropes

defined by the trajectory of dump rope since both bucket and dump rope are assumed to be rigidly connected. This assumption is valid and is based on field observations within the digging phase where these links do not change their orientations. From Fig. 9, it can be noticed that the angular displacement of the dump rope varies more rapidly compared to angular displacements of other ropes, especially at time interval [0, 4] s. This is an important feature for a mining manipulator operated by ropes like a dragline. It means a better orientation of the bucket and a reduction in cycle time, which results in higher productivity. The maximum absolute value of angular displacement of dump rope is 25° at 6 s. This displacement slightly varies after 6 s to avoid spillage of the filled materials from the bucket.

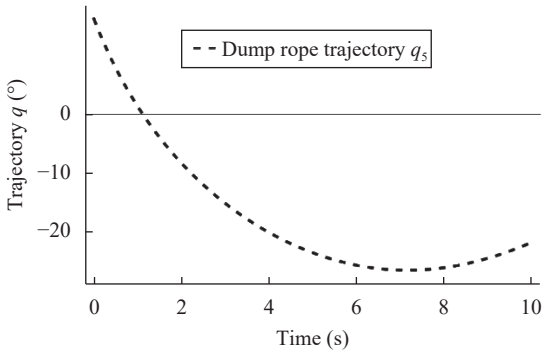

Fig. 9 Dump rope angular displacement

As soon as the bucket is filled, the operator switches the clutches of the hoist and drag motors and engages the swinging motors to rotate the assembly toward dumping area. At this time, the hoist rope retracts and the drag ropes reel out due to inversing the displacements q_7 and q_8. In addition, a sufficient angular displacement of q_1 to the machine house lifts the filled bucket off the ground in a 3D space below the boom. Fig. 10 shows the machine house and its front-end moving the bucket under the effect of three displacements q_1, q_7 and q_8. At the end of full-bucket swinging, the hoist and drag ropes have rotated 25° and 15 s, while the machine house has rotated −80°. As a result, the bucket is positioned below the boom point sheave and the operator is ready to dump the materials in the spoil area.

This work advances the dragline research frontiers by augmenting the number of links in the front-end assembly, applying new kinematics formulation, and by accurately improving the trajectory's measures of every rope. These improvements have a positive impact on the mining industry through understanding the underlying effects of digging scenarios on the dragline rope's endurance and correlating it to the availability and productivity of dragline and the economic useful life of ropes. In other words, selecting appropriate trajectories can help not only increasing productivity with a reduction in the cycle time, but also reduce wear and tear in the wire ropes. As a result, failures in the ropes can be significantly reduced to ensure an efficient and reliable dragline operating system.

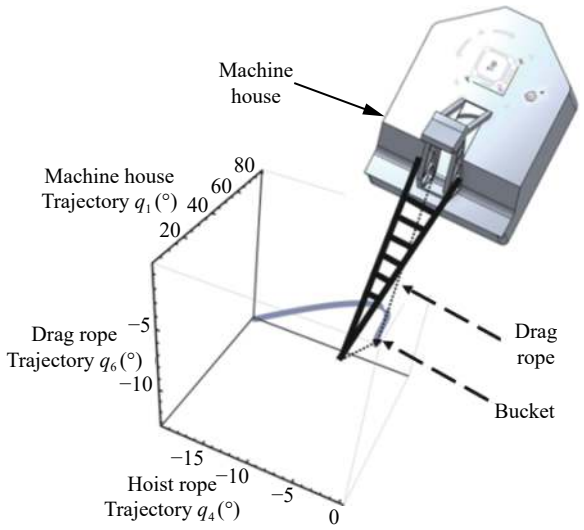

Fig. 10 Bucket trajectory in a 3D space during swinging-back phase

6 Conclusions

Kinematics analysis of closed-loop mechanisms of the dragline is an area of research that has not been studied in detail in literature. Most kinematics mechanisms that have closed-loop structures are solved by splitting the mechanism at joints to convert it into two open chain mechanisms. This results in additional unknowns and makes the analysis lengthy and computationally inefficient. This paper studies the kinematics of a closed-loop system of dragline excavator using the method of generalized speeds. It also forms a basis for performing full multibody dynamic analysis using Kane's method.

The closed-loop dragline front-end assembly is an under-actuated mechanism, which has more degrees of freedom than the number of actuators. The initial conditions search and the inverse kinematics are done by solving the configuration constraint equations using feedforward solution algorithm. Singularity was eliminated by augmenting the Jacobian through coupling the solution algorithm with the Baumgarte's stabilization technique. The kinematics model can produce accurate trajectories of the machine wire ropes and its bucket motion in a 3D operational space. It was shown that no interference is detected between the machine's fixed and moving components. The bucket motion was successfully simulated during digging and full-bucket swinging phase. The kinematics model will be used in the dynamic analysis in a forthcoming paper. It can also serve as a basis for further research in the area of robotics or mechanisms operated by ropes.

Appendix

Table A1 Notion of the elements in the vector loop

$L_0 = \overrightarrow{B_1B_2}.\overrightarrow{b_2}$	Machine house height
$L_1 = \overrightarrow{B^*B_1}.\overrightarrow{b_1}$ $L_2 = -\overrightarrow{B^*B_1}.\overrightarrow{b_2}$	Distance from the first boom pinned point to machine house center of mass COM
$L_3 = \overrightarrow{B^*B_2}.\overrightarrow{b_1}$ $L_4 = \overrightarrow{B^*B_2}.\overrightarrow{b_2}$	Distance from second boom pinned point to the machine house COM
$L_5 = -\overrightarrow{C^*B_2}.\overrightarrow{c_1}$ $L_6 = \overrightarrow{C^*C_1}.\overrightarrow{c_1}$	Distance from boom COM to its end
$L_7 = \overrightarrow{D^*C_1}.\overrightarrow{c_2}$ $L_8 = \overrightarrow{D^*D_1}.\overrightarrow{e_1}$	Sheave-radius R_s
$L_9 = \overrightarrow{F^*E_1}.\overrightarrow{f_1}$ $L_{10} = -\overrightarrow{F^*F_1}.\overrightarrow{f_1}$	Half-length of the dump rope
$L_{11} = \overrightarrow{B_3B^*}.\overrightarrow{b_1}$	Distance from machine house COM to axis of swinging
$L_{12} = \overrightarrow{F^*H_1}.\overrightarrow{f_1}$ $L_{13} = -\overrightarrow{F^*H_1}.\overrightarrow{f_2}$	Distance from dump rope COM to the bucket
$q_7 = \overrightarrow{B_1F_1}.\overrightarrow{g_1}$	Drag rope displacement
$q_8 = \overrightarrow{E_1D_1}.\overrightarrow{e_2}$	Hoist rope displacement
λ	Angle between $\overrightarrow{B_1D}$ and horizontal axis
q_2	Boom angle with horizontal axis

Acknowledgements

The authors are grateful to the anonymous referees for their valuable inputs. The funding from the Robert H. Quenon Endowment at Missouri S&T for this research is also greatly acknowledged.

References

[1] Komatsu Company. Available: https://mining.komatsu/surface-mining/draglines, 2019.

[2] G. Lumley, M. McKee. Mining for Efficiency, Technical Report (Mining Intelligence & Benchmarking), Pricewaterhouse Coopers, Sydney, Australia, 2014.

[3] R. A. Carter. Moving and maintaining the world's biggest diggers. *Engineering & Mining Journal*, vol. 216, no. 11, pp. 40–59, 2015.

[4] A. K. Kemp. Computerized system analyzed dragline performance prints out data. *Coal Age*, vol. 79, no. 9, pp. 92–97, 1974.

[5] C. E. McCoy Jr, L. J. Crowgey. Anti-tightline control system for draglines used in the surface mining industry. In *Proceedings of Conference Record, Industry Applications Society, IEEE-IAS Annual Meeting*, Behrend College Graduate Center, Pennsylvania State University, Pennsylvania, USA, pp. 140–145, 1980.

[6] N. Godfrey, A. Susanto. Partial automation of a dragline working in conjunction with a hopper/crusher/conveyor overburden removal system. In *Proceedings of the 15th Large Open Pit Mining Conference*, Institute of Electrical and Electronics Engineers, New York, USA, 1980.

[7] H. L. Hartman. *Introductory Mining Engineering*, New York, USA: Wiley, Article number 633, 1987.

[8] D. K. Haneman, H. Hayes, G. I. Lumley. Dragline performance evaluations for tarong coal using physical modelling. In *Proceedings of the 3rd Large Open Pit Mining Conference*, The Australasian Institute of Mining and Metallurgy, Mackay, Australia, 1992.

[9] S. W. P. Esterhuyse. The Influence of Geometry on Dragline Bucket Filling Performance, Master dissertation, Stellenbosch University, Stellenbosch, South Africa, 1997.

[10] P. F. Knights, D. H. Shanks. Dragline productivity improvements through short-term monitoring. In *Proceedings of Institution of Engineers, Coal Handling and Utilization Conference*, Sydney, Australia, pp. 100–103, 1990.

[11] P. Corke, J. Roberts, G. Winstanley. Experiments and experiences in developing a large robot mining system. *Experimental Robotics VI*, P. Corke, J. Trevelyan, Eds., London, UK: Springer, pp. 183–192, 2000. DOI: 10.1007/BFb0119397.

[12] J. Roberts, G. Winstanley, P. Corke. Three-dimensional imaging for a very large excavator. *The International Journal of Robotics Research*, vol. 22, no. 7–8, pp. 467–477, 2003. DOI: 10.1177/02783649030227003.

[13] J. Kyle, M. Costello. Comparison of measured and simulated motion of a scaled dragline excavation system. *Mathematical and Computer Modelling*, vol. 44, no. 9–10, pp. 816–833, 2006. DOI: 10.1016/j.mcm.2006.02.015.

[14] T. Yang, N. Sun, H. Chen, Y. C. Fang. Neural network-based adaptive antiswing control of an underactuated ship-mounted crane with roll motions and input dead zones. *IEEE Transactions on Neural Networks and Learning Systems*, to be published. DOI: 10.1109/TNNLS.2019.2910580.

[15] H. J. Yang, M. Tan. Sliding mode control for flexible-link manipulators based on adaptive neural networks. *International Journal of Automation and Computing*, vol. 15, no. 2, pp. 239–248, 2018. DOI: 10.1007/s11633-018-1122-2.

[16] G. W. Zhang, P. Yang, J. Wang, J. J. Sun, Y. Zhang. Integrated observer-based fixed-time control with backstepping method for exoskeleton robot. *International Journal of Automation and Computing*, to be published. DOI: 10.1007/s11633-019-1201-z.

[17] M. Ponnusamy, T. Maity. Recent advancements in dragline control systems. *Journal of Mining Science*, vol. 52, no. 1, pp. 160–168, 2016. DOI: 10.1134/S106273911601025X.

[18] Y. Liu, M. S. Hasan, H. N. Yu. Modelling and remote control of an excavator. *International Journal of Automation and Computing*, vol. 7, no. 3, pp. 349–358, 2010. DOI: 10.1007/s11633-010-0514-8.

[19] X. M. Niu, G. Q. Gao, X. J. Liu, Z. D. Bao. Dynamics and

control of a novel 3-DOF parallel manipulator with actuation redundancy. *International Journal of Automation and Computing*, vol. 10, no. 6, pp. 552–562, 2013. DOI: 10.1007/s11633-013-0753-6.

[20] N. Demirel, S. Frimpong. Dragline dynamic modelling for efficient excavation. *International Journal of Mining, Reclamation and Environment*, vol. 23, no. 1, pp. 4–20, 2009. DOI: 10.1080/17480930802091166.

[21] Y. Li, W. Y. Liu. Dynamic dragline modeling for operation performance simulation and fatigue life prediction. *Engineering Failure Analysis*, vol. 34, pp. 93–101, 2013. DOI: 10.1016/j.engfailanal.2013.07.020.

[22] T. R. Kane, D. A. Levinson. *Dynamics: Theory and Applications*, New York, USA: McGraw-Hill, 1985.

[23] A. K. Banerjee. *Flexible Multibody Dynamics: Efficient Formulations and Applications*, West Sussex, UK: John Wiley and Sons, Ltd, 2016.

[24] M. Wardeh. Computational Dynamics and Virtual Dragline Simulation for Extended Rope Service Life, Ph. D. dissertation, Missouri University of Science and Technology, Rolla, USA, 2018.

[25] J. Baumgarte. Stabilization of constraints and integrals of motion in dynamical systems. *Computer Methods in Applied Mechanics and Engineering*, vol. 1, no. 1, pp. 1–16, 1972. DOI: 10.1016/0045-7825(72)90018-7.

Muhammad A. Wardeh received the B. Eng. degree in mechanical design and production from Damascus University, Syria in 2007. He received two M. Eng. degrees in material science and engineering from the Universities of Paris 6 and 11, France in 2011 and 2012, respectively. He received the Ph. D. degree in mining engineering (engineering mechanics with a focus on computational multibody dynamics and virtual modeling) from Missouri University of Science and Technology (Missouri S&T), USA in 2018. From 2006 to 2009, he worked for multiple engineering firms in China and Europe. From 2010 to 2012, he was a graduate research assistant in a master's program (Master MAGIS Materials and Engineering Sciences in Paris), France. In 2019, he served as a research associate in the Center for Infrastructure Engineering Studies at Missouri S&T, USA.

His research interests include computational dynamics, virtual modeling, finite element analysis, and materials constitutive modeling, microstructural materials modeling and their testing and surface characterization.

E-mail: mawc6f@mst.edu (Corresponding author)
ORCID iD: 0000-0001-6343-2087

Samuel Frimpong received the Ph. D. degree from the University of Alberta, Canada in 1992. He is a professor and the Robert H. Quenon Endowed Chair at Missouri S&T and Director of the Heavy Machinery Research Laboratory. His professional experience includes over 30 years of research and teaching, over 20 years of university administration, and several years of industry practice. He has been recognized with the 2018 Faculty External Recognition Award by Missouri S&T; 2018 Outstanding Faculty of the Year Award by Sigma Chi Fraternity at Missouri S&T; 2017 Daniel C. Jackling Award by Society for Mining, Metallurgy and Exploration (SME); 2010 Missouri S&T Chancellor's Leadership Award; Robert H. Quenon Endowed Chair by Missouri S&T, USA (2004); Distinguished Lecturer Award by Canadian Petroleum Institute (1998–2004); 1997 Award of Distinction by World Mining Congress; University of Alberta/Canadian International Development Agency Ph. D. Scholar (1989–1992); Life Patron of George Grant University of Mines and Technology Alumni Association (2001); 1989 Grand Award by the NW Mining Association, UNESCO Research Fellowship (1986–1988) and State Gold Mining Corporation (SGMC) Gold Scholar (1981–1986). Frimpong is a member of APLU Board on Natural Resources, College of Reviewers for Canada Foundation for Innovation and Canada Research Chairs' Program and ASCE-UNESCO Scientific Committee on Emerging Energy Technologies (ASCE-UNESCO SCEET). He is currently the Editor-In-Chief of the *Journal of Powder Metallurgy and Mining*; Editor-In-Chief of *International Journal of Mining Engineering and Technology*; Editor of *Research and Reports on Metals*; Editorial Board Member for *International Journal of Mining Science*; Editor of the *Journal of MOJ Mining and Metallurgy*; Editorial Board Member for *International Journal of Mining, Reclamation and Environment*; and Associate Editor for *Mining and Minerals Engineering*. He is a registered professional engineer and a member of the Association of Professional Engineers and Geoscientists of Alberta, Canadian Institute of Mining, Metallurgy and Petroleum, The Society for Mining, Metallurgy, and Exploration (SME), American Society of Civil Engineers (ASCE), and Society for Modeling & Simulation International.

His research interests include formation excavation engineering, mine automation and intelligent mining systems, synthetic and renewable energy, machine dynamics and fatigue modeling, and mine safety and health.

E-mail: frimpong@mst.edu